PERGAMON

Planetary and Space Science 48 (2000) 447–462

Planetary and Space Science

www.elsevier.nl/locate/planspasci

Laboratory investigation on the formation of unsaturated nitriles in Titan's atmosphere

N. Balucani[a, 1], O. Asvany[a, 2], Y. Osamura[b], L.C.L. Huang[a], Y.T. Lee[a], R.I. Kaiser[a,*, 2]

[a]*Institute of Atomic and Molecular Sciences, 1, Section 4, Roosevelt Rd., 107, Taipei, Taiwan*
[b]*Department of Chemistry, Rikkyo University, 3-34-1-Nishi-ikebukuro, Toshima-ku, Tokyo, 171, Japan*

Received 24 June 1999; accepted 19 August 1999

Abstract

Crossed molecular beam experiments of ground state cyano radicals, $CN(X^2\Sigma^+)$, with hydrocarbons acetylene (C_2H_2), ethylene (C_2H_4), methylacetylene (CH_3CCH), allene (H_2CCCH_2), dimethylacetylene (CH_3CCCH_3), and benzene (C_6H_6,) were performed to investigate the formation of unsaturated nitriles in Titan's atmosphere. These radical–neutral reactions have no entrance barrier, depict an exit barrier well below the energy of the reactant molecules, and are all exothermic. The CN radical attacks the π electron density at the olefine, alkyne, and aromatic molecules; the formation of an initial addition complex is a common pathway on the involved potential energy surfaces for all reactions. A subsequent carbon–hydrogen bond rupture yields the unsaturated nitriles HCCCN, C_2H_3CN, CH_3CCCN, $H_2CCCH(CN)$, H_2CCCH_2CN, and C_6H_5CN as detected in our experiments. The explicit identification of this CN vs H atom exchange pathway under single collision, makes this reaction-class a compelling candidate to synthesize unsaturated nitriles in Titan's atmosphere. This versatile concept makes it even possible to predict the formation of nitriles once the corresponding unsaturated hydrocarbons are identified in Titan. Here, the C_2H_2 as well as cyanoacetylene, HCCCN, have been already identified unambiguously in Titan's troposphere. Those nitriles as sampled in our crossed beam experiments resemble an ideal challenge to be detected in the framework of the NASA–ESA Cassini–Huygens mission to Titan.

1. Introduction

Saturn's moon Titan is the only solar system body besides Earth with a thick atmosphere. Prior to the Voyager encounters in 1980 and 1981, star occultation and terrestrial based telescopes identified primarily molecular nitrogen, N_2 (90%), and trace gases methane (CH_4) (Karkoschka, 1994; Lunine et al., 1998), ethane (C_2H_6), and acetylene (C_2H_2) in Titan's stratosphere (Thompson et al., 1991). The Voyager missions to Titan opened a new chapter in solar system exploration and extraterrestrial atmospheric chemistry. Ultraviolet, radio-occultation, infrared data identified for the first time numerous minor components like molecular hydrogen, H_2, the hydrocarbon molecules ethylene (C_2H_4), methylacetylene (CH_3CCH), propane (C_3H_8), diacetylene (HCCCCH), monodeuterated methane, CH_3D, the nitriles hydrogen cyanide (HCN), cyanomethane (CH_3CN), dicyan (NCCN), cyanoacetylene (HCCCN), as well as two oxygen-bearing species carbon monoxide (CO) together with carbon dioxide (CO_2) (Letourneur and Coustenis, 1993; Clarke and Ferris, 1995, 1997a,b; Raulin et al., 1990, 1998; Hidayat et al., 1997, 1998; Tanguy et al., 1990, 1998; Lara et al., 1994; Griffith et al., 1998; Kostiuk et al., 1997.

Although Titan's atmosphere is constantly being

* Corresponding author.
E-mail address: kaiser@po.iams.sinica.edu.tw (R.I. Kaiser).
[1] Visiting scientist. Permanent address: Dipartimento di Chimica, Università di Perugia, 06123 Perugia, Italy.
[2] Also: Department of Physics, Technical University Chemnitz-Zwickau, 09107 Chemnitz, Germany.

0032-0633/00/$ - see front matter
PII: S0032-0633(00)00018-0

bombarded with high energy photons and cosmic ray particles as it has been for the last 4.5 billion years, the origin and evolution of the present atmospheric composition is far from resolved. In the upper layers, the energy deposition is mainly from strongly ionizing high energy electrons from the Saturnian magnetosphere and short wavelength solar ultra violet photons ($\lambda < 155$ nm). Hence the ionospheric chemistry is dominated by ion–molecule reactions of predominantly N_2^+ and hydrocarbon ions (Fox and Yelle, 1997; Ewan et al., 1998; Ip 1990; Nagy and Cravens, 1998; Keller et al., 1998). The longer wavelength photons, however, can penetrate down to the stratosphere to photodissociate molecules; hence the chemistry in these atmospheric regions is expected to be driven by neutral–neutral chemistry of photochemically generated radicals with neutral species (Seki et al., 1996; Lellouch, 1990; Lorenz et al., 1997). To simulate this chemistry of Titan's atmosphere in terrestrial laboratories and reproduce the chemical composition as observed in Titan, a multitude of discharge studies, photochemical experiments employing complex gas mixtures, as well as electron bombardments of gaseous targets have been performed, leading to the synthesis of a great variety of nitriles CH_3CN, C_2H_3CN, CH_3CCCN and unsaturated hydrocarbons $C_2H_3C_2H_3$, H_2CCCH_2, C_2H_3CCH, and C_3H_6, see for example Thompson et al. (1991), Nascimento et al. (1998), and references therein. Based on the dominance of atmospheric N_2, and CH_4, most experimentalists and modelers postulate Titan's chemistry to be dominated by $N(^2D)$, CH_2, and CH reactions (Tanguy et al., 1990; Raulin et al., 1998 and references therein; Lara et al., 1991). These experiments, however, are performed under bulk conditions, and reaction products are often analyzed off-line and ex situ. Hence, the detailed chemical dynamics of the reaction are not known, and reaction mechanisms can only be inferred indirectly. Nevertheless, a nitrogen and methane dominated atmosphere does not mean necessarily that these species are primarily involved in the synthesis of the observed trace compounds such as nitriles. For most of these postulated reactions, rate constants are unknown, and if they are known, the reaction products have been investigated in only some cases.

The quantification of stratospheric HCN in the altitude of 100–300 km to mixing ratios of about 3.3_*10^{-7} stimulated the development of more detailed photochemical models of Titan (Tanguy et al., 1990 and references therein). Most importantly, HCN and NCCN can be photolyzed to yield $CN(X^2\Sigma^+)$ radicals. Since the hydrogen cyanide and cyano concentration profiles overlap with atmospheric regions containing unsaturated hydrocarbons such as acetylene, ethylene, and diacetylene (Lellouch, 1990; Rowe and Parent, 1995), these CN radicals might react with olefines and alkynes to unsaturated nitriles. This postulate gains support by the detection of C_2H_2 and the CN precursor C_2N_2 and HCN together with the potential HCCCN reaction products in Titan's troposphere. Recent laboratory studies on CN reactions with unsaturated hydrocarbons at room temperature (Butterfield et al., 1993; Yang et al., 1992; Lichtin and Lin, 1985, 1986; North et al., 1997) and down to temperatures as low as 13 K suggest that these reactions are very fast and hold the rate constants in the order of gas kinetics of about 10^{-10} cm^3s^{-1} (Rowe and Parent, 1995; Smith et al., 1997). The low temperature experiments employed the CRESNU technique co-expanding gas mixtures of the photochemical precursor for the free radical reactant, e.g. NCNO for CN, the coreactant, and the carrier gas through a convergent–divergent Laval nozzle. A pulsed photolysis laser generates the CN radicals whose concentration profile are monitored via laser induced fluorescence to study the kinetics of the CN radical reacting with the hydrocarbon molecules. Although these experiments monitor only the decay kinetics of the free radical fail and thereby fail to identify the products, they demonstrate unambiguously that CN could react under extreme low temperatures with unsaturated hydrocarbons. These limitations clearly indicate the urgency of systematic laboratory studies to identify the reaction products of neutral–neutral encounters relevant to the synthesis of nitriles in Titan's atmosphere.

What experimental technique is suitable to investigate these gas phase reactions? First, experiments must be performed under single collision conditions. This means that in a binary reaction proceeding via a complex, $A + BC \rightarrow [ABC]^* \rightarrow AB + C$, one species A reacts only with one species BC without collisional stabilization or successive reaction of the initially formed $[ABC]^*$ complex (exclusion of three body reactions). This requirement guarantees that the nascent reaction product undergoes no secondary reaction. Second, highly unstable and reactive radicals must be prepared under well defined conditions (internal states, velocity, velocity spread) and reaction products with often unknown spectroscopic properties have to be probed. Hence, the majority of interesting unsaturated nitriles cannot be sampled via optical detection schemes such as laser induced fluorescence (LIF) and resonance enhanced multi photon ionization (REMPI), and a 'universal' detector is crucial. Finally, we have to take into consideration that a variety of structural isomers can contribute to the reaction product. Here, the knowledge of detailed chemical dynamics of a reaction can be employed to elucidate the product isomer(s). In our experiments, we employed the crossed molecular beams technique with a universal mass spectrometric detector, cf Section 2 for a detailed description. This setup represents a versatile tool to: (a) study reaction

products under single collision conditions without three body reactions; (b) investigate the chemical dynamics of radical–neutral reactions; and (c) identify distinct structural isomers relevant to the formation of nitriles in Titan's atmosphere under well-defined reactant conditions. This paper compiles the up-to-date research on crossed-beam reactions of $CN(X^2\Sigma^+)$ radical reactions with acetylene (1), ethylene (2), methylacetylene (3), allene (4), dimethylacetylene (5), and benzene (6) as potential source to form unsaturated nitrile isomers in Titan's troposphere:

$$C_2H_2 + CN \rightarrow HCCCN + H, \quad (1)$$

$$C_2H_4 + CN \rightarrow C_2H_3CN + H, \quad (2)$$

$$\begin{aligned} CH_3CCH + CN &\rightarrow CH_3CCCN + H, \\ &\rightarrow HCCCN + CH_3, \\ &\rightarrow H_2CCCH_3CN + H, \end{aligned} \quad (3)$$

$$\begin{aligned} H_2CCCH_2 + CN &\rightarrow H_2CCCCH_3CN + H, \\ &\rightarrow HCCCH_2CN + H \end{aligned} \quad (4)$$

$$\begin{aligned} CH_3CCCH_3 + CN &\rightarrow H_2CCCCH_3CN + H \\ &\rightarrow CH_3CCCN + H, \\ &\rightarrow CH_3CCCN + CH_3, \end{aligned} \quad (5)$$

$$C_6H_6 + CN \rightarrow C_6H_5CN + H. \quad (6)$$

2. Crossed molecular beam set up

The 35″ crossed molecular beam machine consists of two source chambers fixed at a 90° crossing angle, a stainless steel scattering chamber, and an ultra high vacuum tight, rotatable triply differentially pumped quadrupole mass spectrometric detector, cf Figs. 1 and 2. The scattering chamber is evacuated by oil free turbo molecular pumps to about 10^{-7} mbar and operated at typically 10^{-6} mbar during the reactive scattering experiments. In the primary source, a pulsed supersonic cyano $CN(X^2\Sigma^+)$ radical beam is generated in situ by laser ablation of graphite and subsequent seeding of the liberated species in molecular nitrogen which also serves as a reactant. In detail, a Nd:YAG laser operates at 30 Hz repetition rate at 266 nm which is generated by two doubling crystals from the 1064-nm laser output. The output power was limited

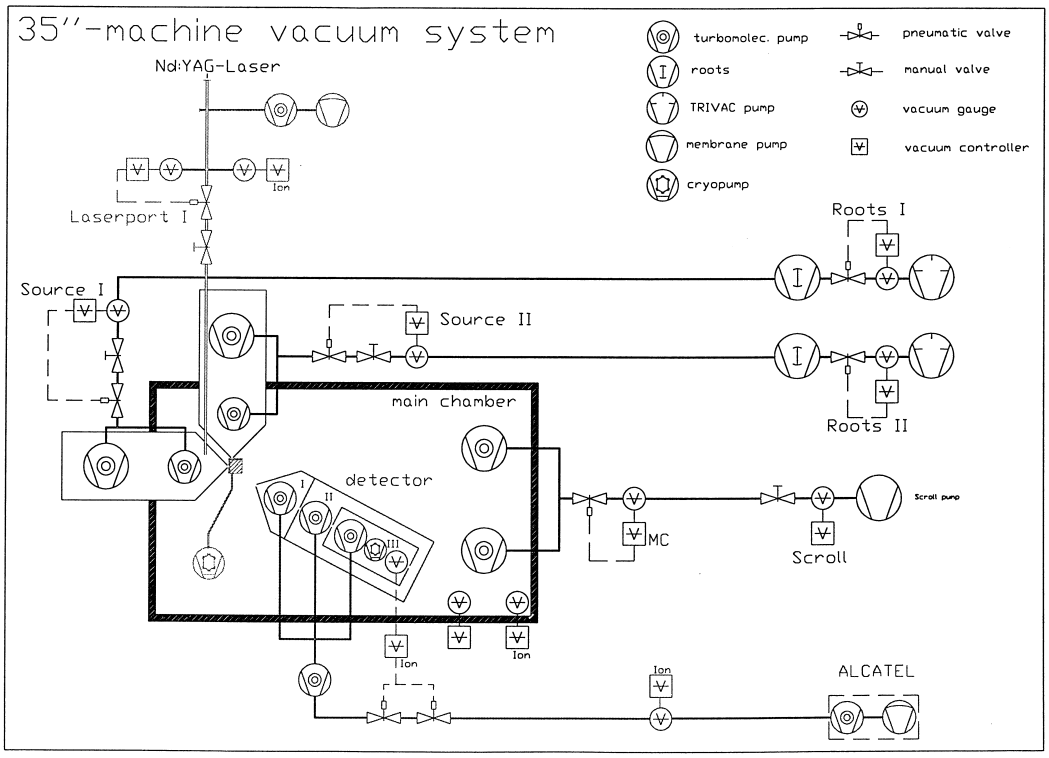

Fig. 1. Schematic representation of the 35″ crossed molecular beams machine.

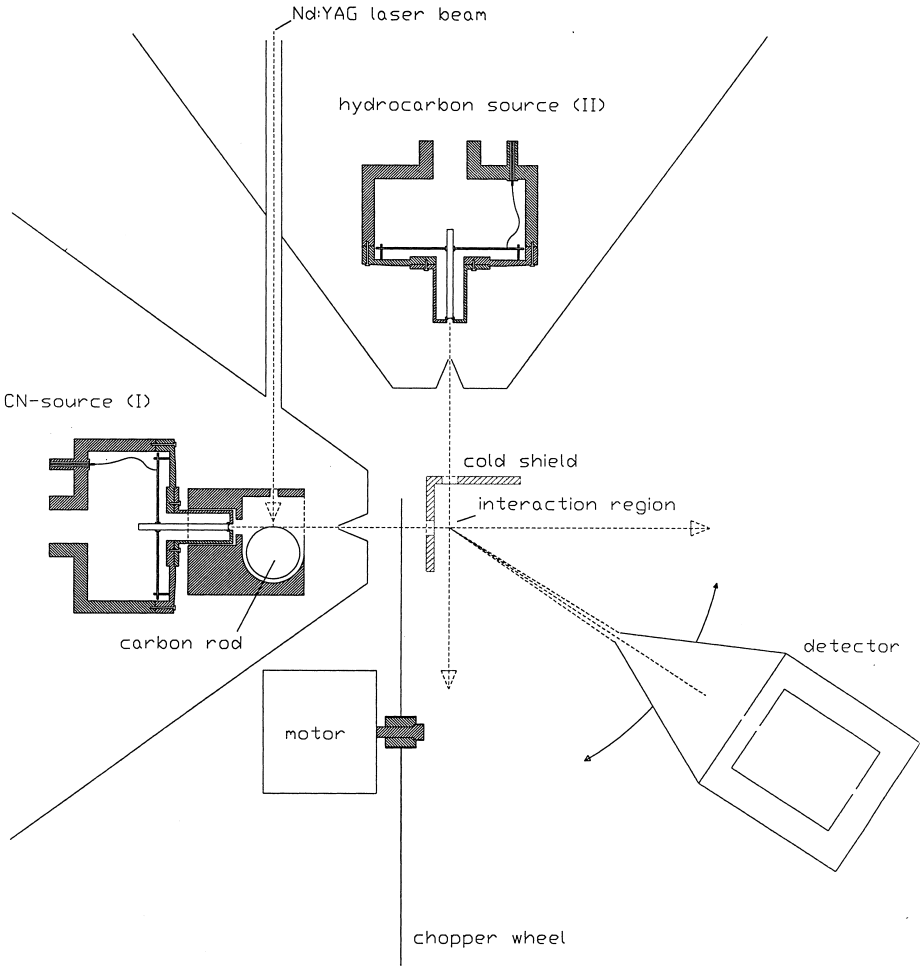

Fig. 2. Schematic top view of the source chambers, chopper wheel, and interaction region.

to a maximum of 30 mJ per pulse to avoid generation of vibrationally excited CN radicals which might show different reaction dynamics compared to CN in its vibrational ground state (Kaiser and Suits 1995; Kaiser et al., 1999). We guided the laser beam via a differentially pumped laser port into the vacuum system and focused it very tightly onto a rotating carbon rod. The ablated carbon species were seeded into nitrogen carrier gas released by a pulsed valve at 4 atm backing pressure operating at 60 Hz and 80 μs opening time. The valve is placed 7 mm in front of the graphite rod and is oriented perpendicular to the laser beam. The in situ generated CN radicals pass though a skimmer into the main chamber of the machine. A four slot chopper wheel is located after the skimmer and rotates at 240 Hz. It selects a 9 μs slice of well-defined velocity and speed ratio from the pulsed beam which reaches the interaction region. At this point, the CN radicals collide at a right angle with the second pulsed beam of the unsaturated hydrocarbons at collision energies between 21.0 and 30.5 $kJmol^{-1}$. Here, the velocity of the CN beam is chosen to be between 900 and 1930 ms^{-1}, and the hydrocarbon beams between 740 and 900 ms^{-1}. The secondary pulsed valve is operated at 80 μs and 60 Hz with backing pressures between 460 and 600 torr depending on the gas. Each experiment must avoid any reaction of CN radicals with hydrocarbon clusters present in the slower part of the secondary beam. Hence extreme care has to be given to choose the correct time delay between both pulsed valves. In our experiments, the second pulsed valve opens at about 10–60 μs — dependent on the velocity of the reactant gas — prior to the primary pulsed valve to allow the fast part of the hydrocarbon beam to react with the CN pulse.

Reactively scattered species are registered by a triply differentially pumped detector consisting of a liquid nitrogen cooled electron impact ionizer followed by a quadrupole mass detector, and a Daly type detector. This set up is rotatable between -25.0° and 72.0° in the scattering plane as defined by both beams. As the ionized and mass selected species hit the surface of the

detector, it emits an electron cascade which hits an organic scintillator mounted outside the detector chamber to generate a photon cascade and hence an electric pulse. Each pulse is amplified and passes a discriminator to eliminate low-level noise. This signal is fed into the multi-channel scaler which records the time of flight spectra of the arriving ions. Despite the triply differential pumping set up, molecules desorbing from wall surfaces lying on a straight line to the electron impact ionizer cannot be avoided. Their mean free path is in the order of 10^3 m compared to maximum detector dimensions of about 1 m. To reduce this background, a copper plate attached to a two stage closed cycle helium refrigerator is placed right before the collision center and cooled down to 4.5 K. Thus, the ionizer views a cooled surface which traps all the species with the exception of molecular hydrogen and helium.

3. Data analyses

For the physical interpretation of the reactive scattering data it is crucial to transform the laboratory data into the center-of-mass (CM) system, Fig. 3. For simplicity, this study considers the bimolecular reaction $A+BC \rightarrow AB+C$. However, if this observer dwells at the CM, the CM is at rest. Fig. 3 shows the relation between both reference frames. In the experiment, a beam of species A with a laboratory velocity **v(A)** crosses a beam of species BC with a laboratory velocity **v(BC)** perpendicularly giving the relative velocity **g** of A with respect to BC to

$$\mathbf{g} = \mathbf{v}(\mathbf{A}) - \mathbf{v}(\mathbf{BC}). \tag{7}$$

In the laboratory system, the center of mass frame moves with the velocity **v(CM)** calculated with the masses of the reactants m(A) and m(BC) to

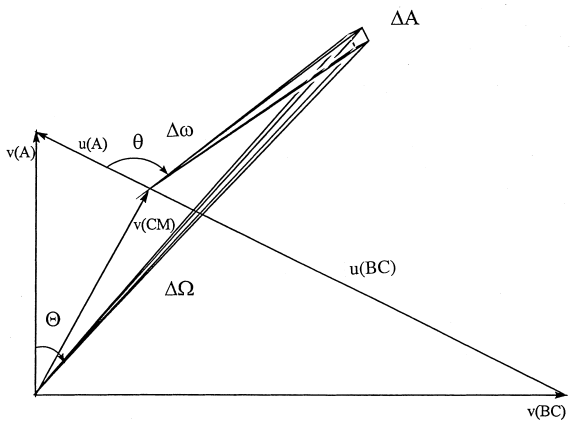

Fig. 3. Relation between the laboratory and center-of-mass reference frames.

$$\mathbf{v}(\mathbf{CM}) = (\mathrm{m(A)}\mathbf{v}(\mathbf{A}) + \mathrm{m(BC)}\mathbf{v}(\mathbf{BC}))/(\mathrm{m(A)} + \mathrm{m(BC)}). \tag{8}$$

The center of mass velocity vector divides **g** into two sections, the velocity of A and BC in the center of mass frame, **u(A)** and **u(BC)**, respectively. The magnitude of these vectors is inversely proportional to the mass ratio of the reactants. To convert the laboratory data to the center of mass system, we employ a forward-convolution routine to fit the TOF spectra $I(\Theta,t)$ at different laboratory angles Θ and the product angular distribution in the laboratory frame (LAB). This procedure initially guesses the angular flux distribution $T(\theta)$ and the translational energy flux distribution $P(E_T)$ in the CM frame assuming mutual independence. Here, θ defines the scattering angle in the CM system measured from the A beam and E_T the CM translational energy. Then, TOF spectra and LAB distribution were calculated from these $T(\theta)$ and $P(E_T)$ accounting for the velocity and angular spread of both beams, the detector acceptance angle, and the ionizer length. Both $T(\theta)$ and $P(E_T)$ are refined until a reasonable fit of the experimental data is achieved.

In detail, four transformation steps are necessary. First, we transform the $I(\Theta,t)$ time domain to the velocity domain recalling that

$$I(\Theta, t)\,\mathrm{d}t = I(\Theta, v)\,\mathrm{d}v \tag{9}$$

and

$$\frac{\mathrm{d}v}{\mathrm{d}t} = -\frac{v^2}{L} \tag{10}$$

with the velocity v and neutral flight length L. This gives

$$I(\Theta, t) = -I(\Theta, v)v^2/L. \tag{11}$$

Second, the detector analyzes number density, whereas $T(\theta)$ and $P(E_T)$ represent flux distributions. Hence we have to transform a number density distribution (molecules cm^{-3}) to a flux distribution (molecules cm^{-1} s^{-1}). Here, the product of $I(\Theta, v) * v$ is nothing else but a flux distribution in the lab frame defined as $\sigma(\Theta,v)$, yielding:

$$I(\Theta, t) = -\sigma(\Theta, v)v/L. \tag{12}$$

Third, we have to transform $\sigma(\Theta,v)$ to the CM flux distribution $\sigma(\theta,u)$ with the velocity u of the product. The v^2/u^2-transformation Jacobian can be derived by considering the cross-section proportional flux per unit time in a solid angle to be constant in the laboratory and CM frame:

$$\sigma(\Theta, v)\Delta\Omega = \sigma(\theta, u)\Delta\omega \tag{13}$$

where $\Delta\Omega$ is the solid angle sustained by the detector

aperture ΔA in the laboratory, and the solid angle $\Delta\omega$ in the CM frame. Recalling the definition of a solid angle, i.e. $d\Omega = dA/r^2$ with the defining aperture of area dA at a distance r from the interaction region and $\Delta\Omega = \Delta A/(v*t)^2$ and $\Delta\omega = \Delta A/(u*t)^2$, we plug these equations into (13), to obtain the transformation Jacobian. Now, we yield

$$I(\Theta, t) = -\sigma(\theta, u)v^3/L/u^2. \quad (14)$$

The fourth step transforms the velocity distribution to the total translational energy distribution using energy and momentum conservation — with $\bar{\mu} = m_{AB}(m_{AB}/m_C + 1)$ and the masses of the products AB and C — to

$$\sigma(\theta, u) = \sigma(\theta, E_T) * \bar{\mu} * u. \quad (15)$$

yielding

$$I(\Theta, t) = -\sigma(\theta, E_T) * \bar{\mu}\ v^3/L/u. \quad (16)$$

Here, $\sigma(\theta,E_T)$ is the double differential cross-section in the CM reference frame. $\sigma(\theta,E_T)$ is proportional to $T(\theta)$ and $P(E_T)$, hence

$$\sigma(\theta, E_T) = C * T(\theta) * P(E_T) \quad (17)$$

with a constant C. Since $T(\theta)$ and $P(E_T)$ are normalized, C is obtained by integrating $\sigma(\theta,E_T)$ over θ, φ — the angle around the relative velocity vector **g** — and E_T:

$$\sigma(E) = \int_0^{\infty}\int_0^{2\pi}\int_0^{\pi} P(E_T)T(\theta)\ \sin\ \theta\ d\theta\ d\varphi\ dE_T = C. \quad (18)$$

This identifies C as the total cross-section of the bimolecular reaction $A + BC \rightarrow AB + C$ at a collision energy E. Hence, the final relation between the TOF spectra at a laboratory angle Θ, $I(\Theta,t)$, and the iteratively refined CM flux distributions $T(\theta)$ and $P(E_T)$ with the constant C' is given to

$$I(\Theta, t) = C' * T(\theta) * P(E_T) * v^3/u. \quad (19)$$

The ultimate output data of our experiments is the generation of a product flux contour map which reports the differential cross-section (the intensity of the reactively scattered products), $I(\theta, u) \sim P(u) * T(\theta)$, as the intensity as a function of angle θ and product center-of-mass velocity u. This map serves as an image of the reaction and contains all the information of the scattering process.

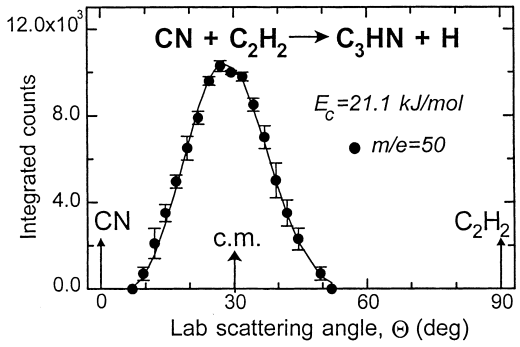

Fig. 4. Laboratory angular distribution for the $CN(X^2\Sigma^+) + C_2H_2$ reaction of the C_3HN product at a collision energy of 21.1 $kJmol^{-1}$.

4. Experimental results

4.1. Laboratory angular distribution (LAB), and TOF spectra

In all crossed beam experiments (1)–(6) we detected the CN vs H exchange channel. Reactive scattering signal was observed at mass to charge ratios m/e = 51 (C_3HN, reaction (1)), m/e = 53 (C_3H_3N, reaction (2)), m/e = 55 (C_4H_3N, reactions (3) and (4)), m/e = 79 (C_5H_5N, reaction (5)), and m/e = 103 (C_7H_5N, reaction (6)). TOF flight spectra of lower m/e ratios down to the bare carbon–nitrogen ion core (m/e = 50 (reactions (1) and (2)), m/e = 62 (reactions (3) and (4)), m/e = 74 (reaction (5)), and m/e = 98 (reaction (6)) were taken at selected angles as well, but show identical pattern and could be fit with the same center-of-mass functions as the parent ion. This finding indicates that those m/e ratios originate in the cracking of the parent in the electron impact ionizer. We like to point out that despite an intensive search, no radiative association channel to the adduct molecule was found experimentally. Likewise, we were not able to identify any CH_3 loss channel in reactions (3) and (5).

Figs. 4–9 present the experimental laboratory pro-

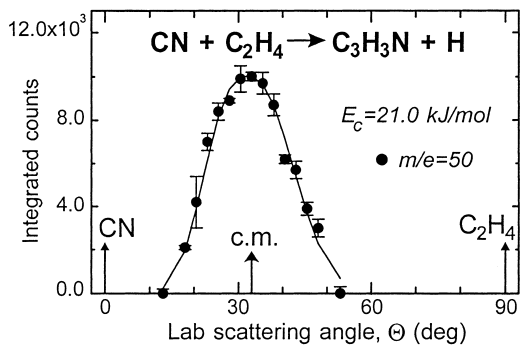

Fig. 5. Laboratory angular distribution for the $CN(X^2\Sigma^+) + C_2H_4$ reaction of the C_2H_3CN product at a collision energy of 21.0 $kJmol^{-1}$.

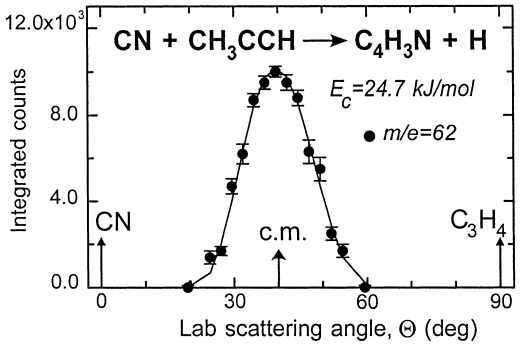

Fig. 6. Laboratory angular distribution for the $CN(X^2\Sigma^+)+CH_3CCH$ reaction of the C_4H_3N isomer at a collision energy of 24.7 kJmol^{-1}.

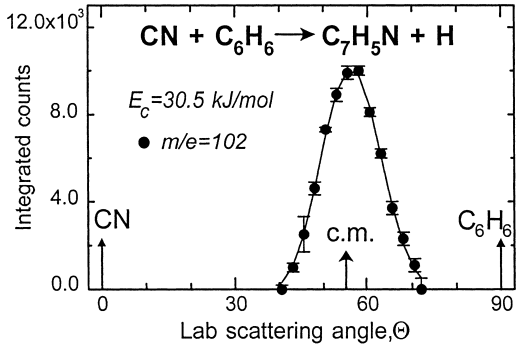

Fig. 9. Laboratory angular distribution for the $CN(X^2\Sigma^+)+C_6H_6$ reaction of the C_6H_5CN isomer at a collision energy of 30.5 kJmol^{-1}.

duct angular distributions and the calculated curves using the center-of-mass best fit functions. The corresponding TOF spectra of the products are shown for selected angles in Figs. 10–15. All our laboratory distributions peak close to the center-of-mass angles, are very narrow, and extend only between 32° and 45° in the scattering plane. Since our quadrupole mass spectrometer cannot discriminate the product isomers explicitly, we must have a closer look at the kinematics and chemical reaction dynamics and the flux contour maps, cf Figs. 16–21. If the energetics of the product isomers are well separated, it is possible to identify the product isomer. For simplicity, let us assume one product can have only two structural isomers I1 and I2. Let's assume further, that isomer I1 is more stable than I2 by 200 kJmol^{-1}. In this case, the reaction to I1 is expected to be more exothermic, and hence the reactive scattering product can be spread into a larger scattering range than I2. In other words, the center-of-mass velocity u_{BC} of the products is different in both

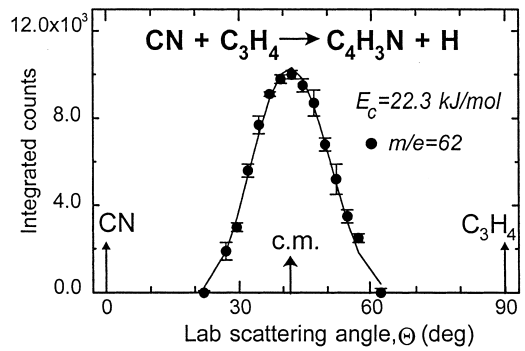

Fig. 7. Laboratory angular distribution for the $CN(X^2\Sigma^+)+H_2CCCH_2$ reaction of the C_4H_3N isomer at a collision energy of 22.3 kJmol^{-1}.

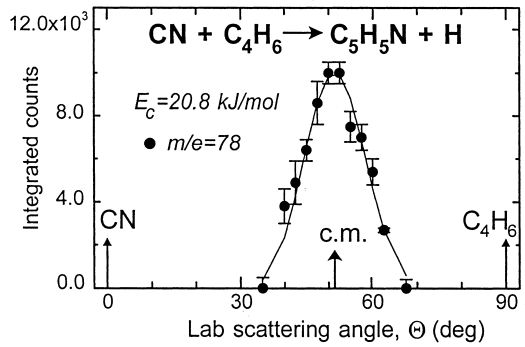

Fig. 8. Laboratory angular distribution for the $CN(X^2\Sigma^+)+CH_3CCCH_3$ reaction of the C_5H_5N isomer at a collision energy of 20.8 kJmol^{-1}.

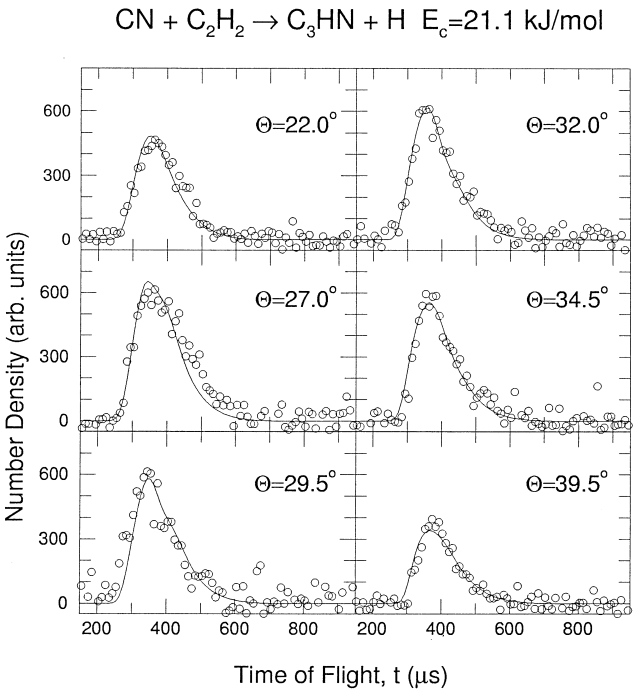

Fig. 10. Time-of-flight data of distinct laboratory angles as indicated in Fig. 4. The dots indicate the experimental data, the solid lines the calculated fit.

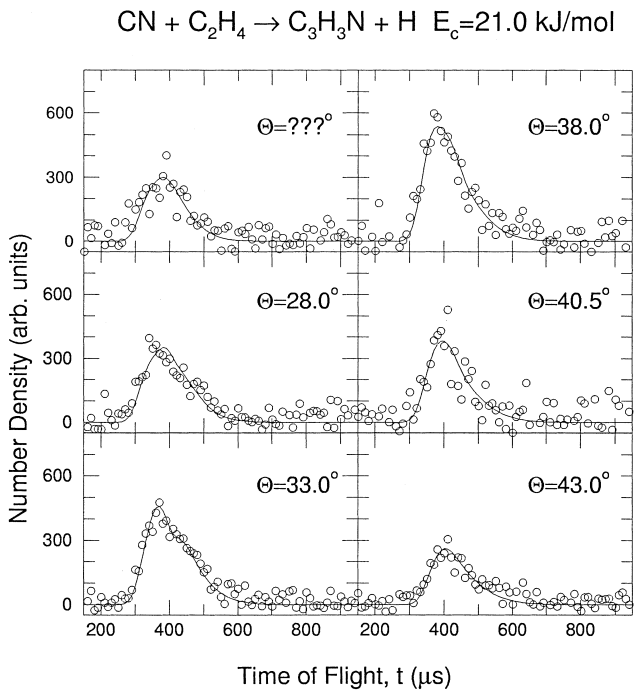

Fig. 11. Time-of-flight data of distinct laboratory angles as indicated in Fig. 5. The dots indicate the experimental data, the solid lines the calculated fit.

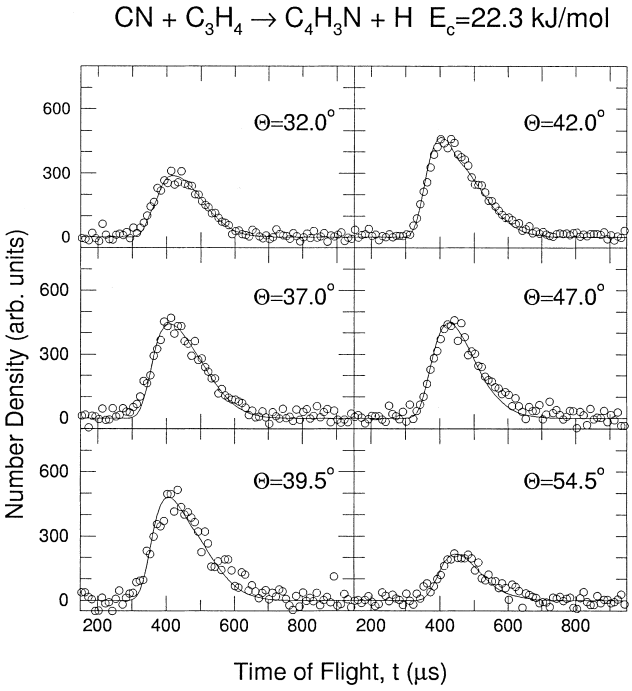

Fig. 13. Time-of-flight data of distinct laboratory angles as indicated in Fig. 7. The dots indicate the experimental data, the solid lines the calculated fit.

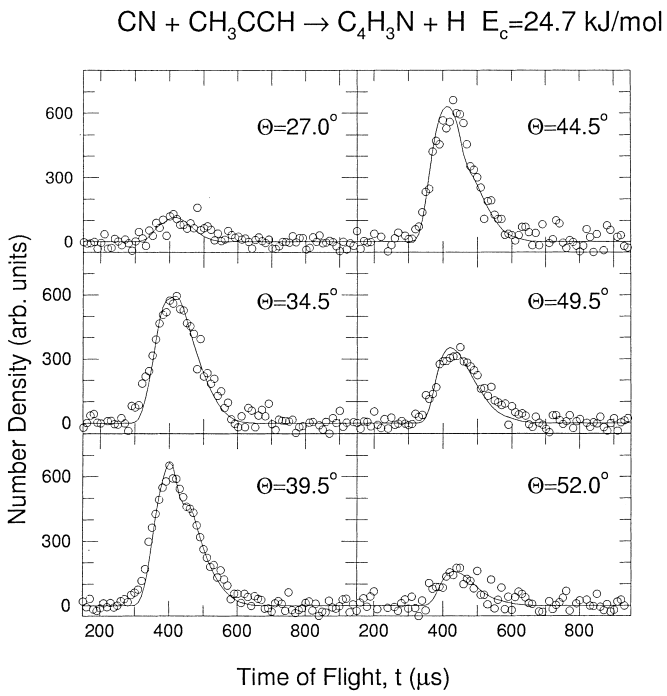

Fig. 12. Time-of-flight data of distinct laboratory angles as indicated in Fig. 6. The dots indicate the experimental data, the solid lines the calculated fit.

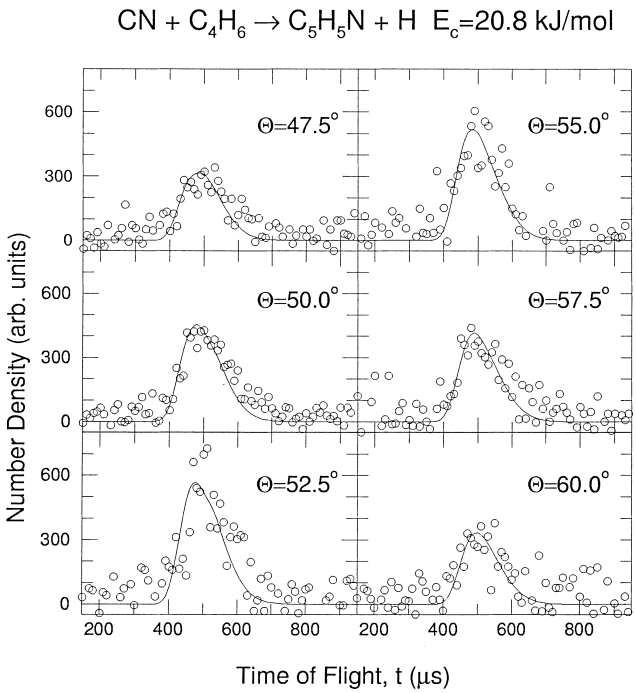

Fig. 14. Time-of-flight data of distinct laboratory angles as indicated in Fig. 8. The dots indicate the experimental data, the solid lines the calculated fit.

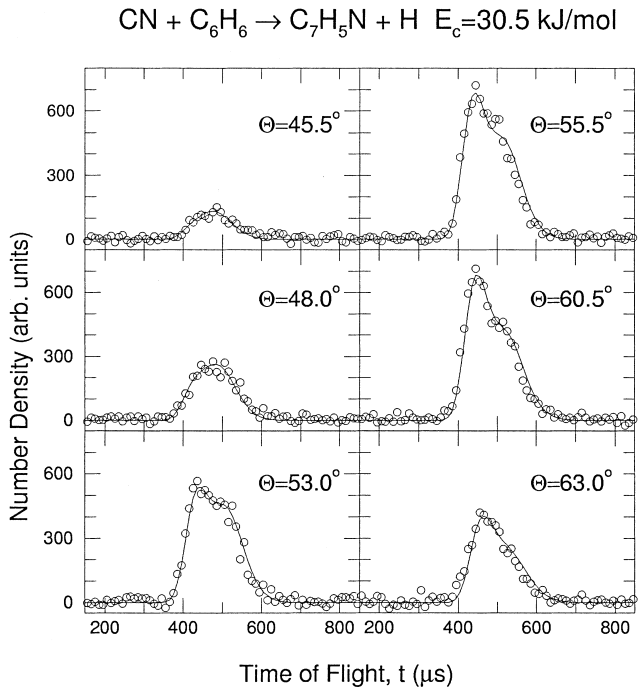

Fig. 15. Time-of-flight data of distinct laboratory angles as indicated in Fig. 9. The dots indicate the experimental data, the solid lines the calculated fit.

cases. This translates in a larger 'Newton circle' for isomer I1 than for I2. These scattering ranges can then be compared with experimentally and theoretically available reaction energies. Here, we find that at least the products cyanoacetylene, HCCCN (reaction (1)), vinylcyanide, C_2H_3CN, reaction (2), 1,1-cyanomethylallene ($CH_3CNCCCH_2$, reaction (5)), and cyanobenzene (C_6H_5CN, reaction (6)) are formed. In case of reactions (3) and (4), the energetically accessible iso-

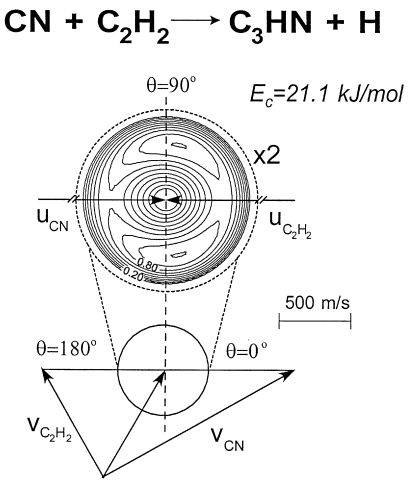

Fig. 16. Velocity flux contour map in the center-of-mass reference frame together with the most probable Newton diagram for the reaction $CN(X^2\Sigma^+) + C_2H_2$ at a collision energy of 21.1 kJmol^{-1}.

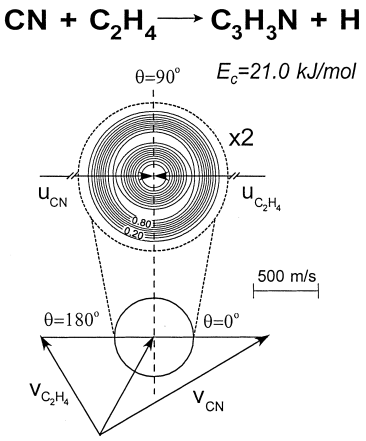

Fig. 17. Velocity flux contour map in the center-of-mass reference frame together with the most probable Newton diagram for the reaction $CN(X^2\Sigma^+) + C_2H_4$ at a collision energy of 21.0 kJmol^{-1}.

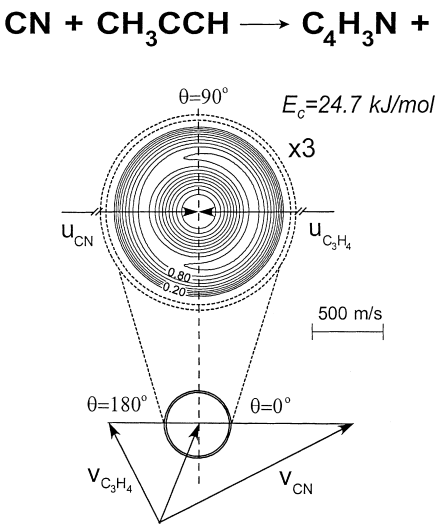

Fig. 18. Velocity flux contour map in the center-of-mass reference frame together with the most probable Newton diagram for the reaction $CN(X^2\Sigma^+) + CH_3CCH$ at a collision energy of 24.7 kJmol^{-1}.

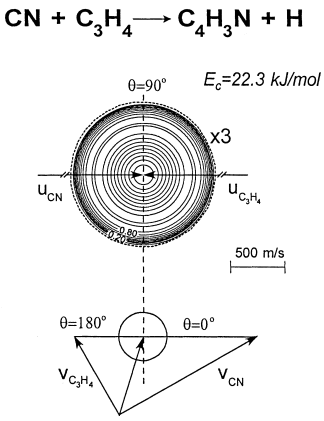

Fig. 19. Velocity flux contour map in the center-of-mass reference frame together with the most probable Newton diagram for the reaction $CN(X^2\Sigma^+) + H_2CCCH_2$ at a collision energy of 22.3 kJmol^{-1}.

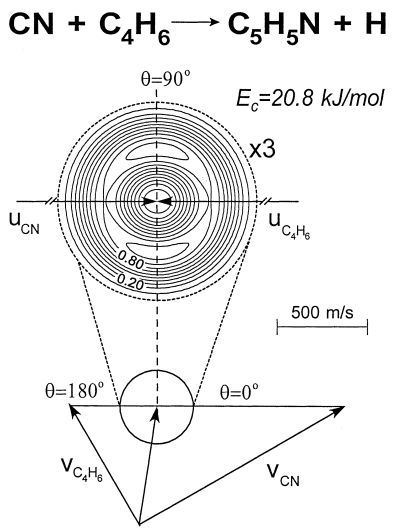

Fig. 20. Velocity flux contour map in the center-of-mass reference frame together with the most probable Newton diagram for the reaction $CN(X^2\Sigma^+)+CH_3CCCH_3$ at a collision energy of 20.8 kJmol^{-1}.

mers cyanoallene ($CNHCCCH_2$) and cyanomethylacetylene (CH_3CCCN) are only separated by about 15–20 kJmol^{-1}, and hence cannot be discriminated yet. In case of reaction (3), we redid the crossed beam experiments with the partially deuterated methylacetylene, CD_3CCH, and found a H atom as well as D atom loss channel. This strongly indicates that both isomers CH_3CCCN and $H_2CCCHCN$ are formed in reaction (3), cf Discussion Section.

4.2. Energetical information from center-of-mass flux contour maps, $I(\theta,u)$

Figs. 16–21 present the center-of-mass flux contour maps $I(\theta,u)$. To get a picture on the energetics, we must have a closer look at the center-of-mass velocity u of the products; here, all the information we gain from u translates to information on the translational energy and $P(E_T)$. To elucidate the chemical reaction dynamics, three properties of the $I(\theta,u)$ are worthwhile studying. First, if the energetics of the product isomers are well separated, the maximum translation energy E_{max} can be used to identify the nature of the products. Here, E_{max} is simply the sum of the reaction exothermicity obtained either from electronic structure calculations or literature and the collision energy in our experiments. Therefore, if we subtract the collision energy from the experimentally determined E_{max} we simply get the exothermicity of the reaction. Best fits of our TOF spectra and LAB distributions were achieved with $P(E_T)$s extending to $E_{max}=100$–130 kJmol^{-1} (reaction (1)), 110–120 kJmol^{-1} (reaction (2)), 90–130 kJmol^{-1} (reaction (3)), 105–110 kJmol^{-1} (reaction (4)), 90–130 kJmol^{-1} (reaction (5)), and 110–115 kJmol^{-1} (reaction (6)). Correcting for the collision energy reactions (1)–(6) must be exothermic by 80–110, 90–100, 65–110, 85–95, 70–110, and 80–90 kJmol^{-1}. Second, in the most favorable case, the distribution maximum of the $P(E_T)$ can give the order-of-magnitude of the barrier height in the exit channel. In general, the $P(E_T)$s show maxima between 15 and 40 kJmol^{-1}. These data suggest a significant geometry as well as electron density change from the decomposing complex to the products resulting in a repulsive bond rupture from a tight transition state. Third, the fraction of energy released into translational degrees of freedom of 30–35% in our systems suggests that the chemical reaction dynamics are governed by an initial collision complex formation, i.e. a covalently bound intermediate from reaction of the unsaturated hydrocarbon with the CN radical. This has very important implications to planetary chemistry. In our crossed beams reactions, the life time of these intermediates is in the order of 10^{-12} s; due to our single collision conditions, a third body collision cannot stabilize this internally excited intermediate. In denser planetary atmospheres, however, this three-body-reaction could take place to give a radical reaction product as well. The explicit identification of these intermediates will be carried out in the next sections.

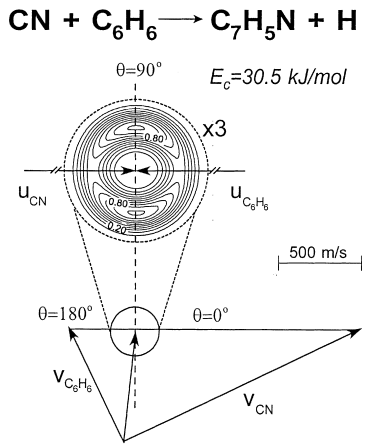

Fig. 21. Velocity flux contour map in the center-of-mass reference frame together with the most probable Newton diagram for the reaction $CN(X^2\Sigma^+)+C_6H_6$ at a collision energy of 30.5 kJmol^{-1}.

4.3. Angular information from center-of-mass flux contour maps, $I(\theta,u)$

The angular information of the flux contour maps gives information on the $T(\theta)$ and is of fundamental importance to elucidate the chemical reaction dynamics on the reactions of CN radicals with unsaturated hydrocarbons (Levine and Bernstein, 1987, and references therein). These graphs show the angular dependent flux distribution an observer would see if he

moves with the center of mass velocity dwelling on the center-of-mass of the system. Here, the direction of the CN beam is defined as 0°, and of the hydrocarbon beam to 180°. Several shapes of the flux distributions are feasible. First, the $T(\theta)$ and corresponding flux contour map $I(\theta,u)$ shows a symmetric profile around 90°, this means the intensity of the flux distribution is the same at a center of mass angle θ and $180°-\theta$. This 'forward–backward' symmetric behavior is characteristic for a bimolecular reaction $A+BC \rightarrow AB+C$ which goes through a $[ABC]^*$ intermediate (indirect scattering dynamics) holding a lifetime larger than its rotation period. Alternatively, a symmetric distribution around 90° could be interpreted in a way that the reaction proceeds though a 'symmetric' exit transition state. In this case, the decomposing complex must have a rotation axis which interconverts the leaving hydrogen atoms. Based on this, the H atom can be released into θ and $180°-\theta$ with equal probability to result in a forward–backward symmetric flux distribution; no information on the lifetime of the fragmenting intermediate can be obtained. We like to point out that the actual interpretation of the $T(\theta)$ goes further. While the symmetry is an essential requirement, the shape of the $T(\theta)$ is determined by the disposal of the total angular momentum and a variety of shapes are indeed possible depending on the correlation between initial and final angular momentum $\mathbf{L}$ and $\mathbf{L}'$, as well as the final rotational angular momentum $\mathbf{j}'$. The final recoil velocity vector, $\mathbf{v}'$, is in a plane perpendicular to $\mathbf{L}'$ and therefore, when the rotational excitation of products is significant, $\mathbf{v}'$ is not in a plane perpendicular to $\mathbf{J}$. When $\mathbf{j}'$ is not zero, the probability distribution for the scattering angle θ, which is the center-of-mass angle between the initial relative velocity $\mathbf{v}$ and $\mathbf{v}'$, depends on the values of J, M and M' where M and M' are the projections of $\mathbf{J}$ on the initial and final relative velocity, respectively. For instance, if the complex dissociates preferentially with low M' values, the final velocity $\mathbf{v}'$ is almost perpendicular to $\mathbf{J}$ and therefore $\mathbf{v}'$ and $\mathbf{v}$ are almost parallel; in this case, the product intensity will be mainly confined to the poles, $\theta=0°$ and $\theta=180°$, similarly to the case of no product rotational excitation, and the center-of-mass angular flux distribution shows maxima at 0° and 180°. On the contrary, when the collision complex dissociates mainly with high M' values, the final relative velocity will be almost parallel to $\mathbf{J}$ and perpendicular to $\mathbf{v}$ and the products will be preferentially scattered at $\theta=90°$ to yield a peak in the center-of-mass angular distribution at 90°. If a light atom such as atomic hydrogen is emitted, and the final angular momentum is much smaller than the final rotational momentum, an isotropic, i.e. flat, $T(\theta)$ is observed. Usually, a distribution of M' values is possible; in some cases, however, the geometry of the decomposing complex may imply a most probable M' value.

Secondly, the angular flux distribution can be asymmetric around 90°; in most cases, the flux at 0° is larger than at180°. In the most simple scenario, this suggests a so called 'osculating complex model': here, the reaction is still indirect and proceeds via complex formation, but the lifetime of the decomposing intermediate is in the order of the rotation period, and multiple rotations cannot occur (case 1). Another optional interpretation of this shape is that the chemical dynamics are governed by two micro channels, i.e. a forward–backward symmetric one, and a second, more forward scattered contribution (case 2). Increasing the collision energy and observing the change in the center-of-mass angular distribution might help to discriminate between both cases. In many experiments, a transition from a forward–backward symmetric to a more forward distribution with increasing collision energy can be connected to an osculating complex model, whereas the reverse trend. i.e. a less pronounced forward peaking as the collision energy rises, supports case 2.

Thirdly, the center-of-mass angular flux distribution can show predominantly flux only in the forward direction, i.e. the flux peaks at 0° and is zero at larger angles, or only in the backward direction, i.e. the flux distribution shows a maximum at 180° and falls down to zero at lower angles. In these cases, the reaction is 'direct' and proceeds either via a very short lived, highly rovibrationally excited intermediate with a lifetime in the order of 0.01 ps, or goes through a transition state $[ABC]^{\#}$ without involving an $[ABC]^*$ complex. We like to recall that a transition state $[ABC]^{\#}$ cannot be isolated in a three body reaction and hence not in Titan's atmosphere; only $[ABC]^*$ complexes can react with a third body to divert the excess energy.

Based on these considerations and Figs. 16–27, it is obvious that all reactions (1)–(6) proceed via indirect scattering dynamics and involve a collision complex. Here, intensity in the flux distribution as well as contour plot is found at 0° and 180°, strongly suggesting that a complex formation takes place. A non-complex (or short lived) complex formation would have resulted in a lacking intensity at the poles. This is clearly not observed in our experiments. Further, reactions (2) and (4)–(6) depict symmetric distributions, and the lifetime of the complex must be longer than the rotational period which is often in the order of pico seconds; since none of the intermediates holds a proper rotation axis, a 'symmetric exit transition state' as discussed before is not involved. We like to point out that in principle, all these collision complexes can be isolated in denser media such as the atmosphere of Titan and contribute directly to the chemistry in the troposphere.

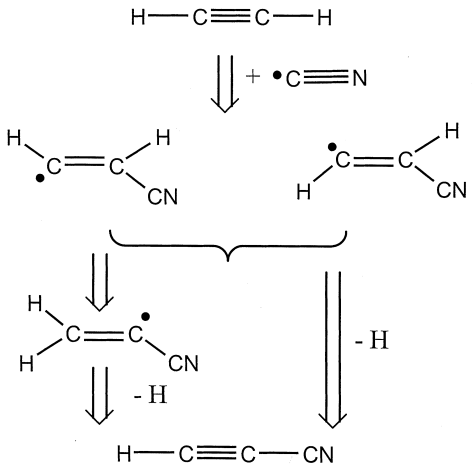

Fig. 22. Schematic representation of the reaction for the reaction $CN(X^2\Sigma^+)+C_2H_2$.

In reactions (1) and (3), the distribution shows an asymmetry and depicts a broad peak around 60–80°. Since our data of these systems show the forward–backward asymmetry becomes more pronounced as the collision energy increases and the intensity growths in forward direction with rising collision energy, an osculating complex is very likely to be formed.

5. Discussion

5.1. C_2H_2 + CN reaction

The spin densities indicate that the unpaired electron

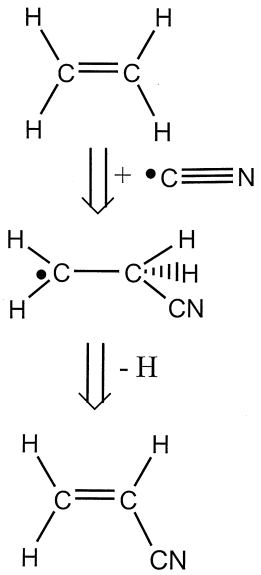

Fig. 23. Schematic representation of the reaction for the reaction $CN(X^2\Sigma^+)+C_2H_4$.

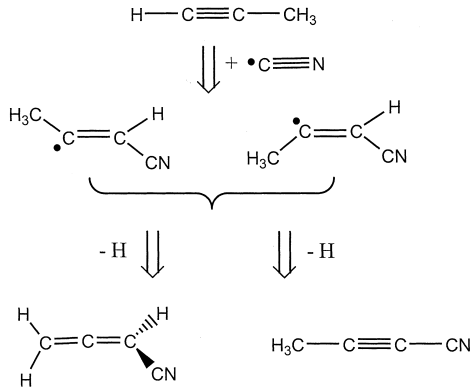

Fig. 24. Schematic representation of the reaction for the reaction $CN(X^2\Sigma^+)+CH_3CCH$.

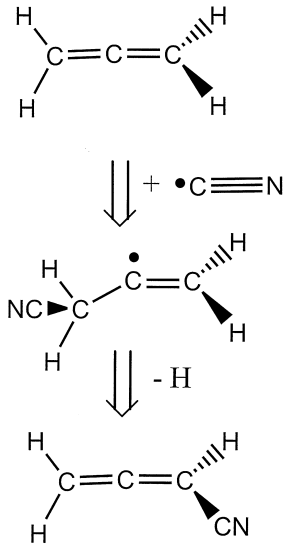

Fig. 25. Schematic representation of the reaction for the reaction $CN(X^2\Sigma^+)+H_2CCCH_2$.

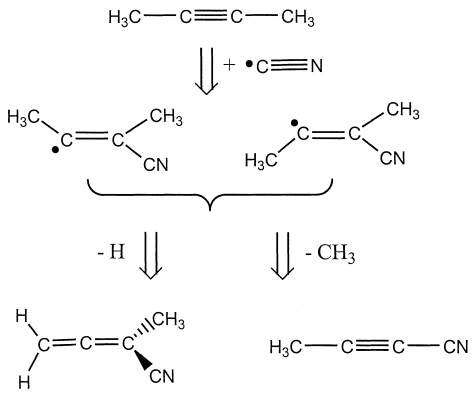

Fig. 26. Schematic representation of the reaction for the reaction $CN(X^2\Sigma^+)+CH_3CCCH_3$.

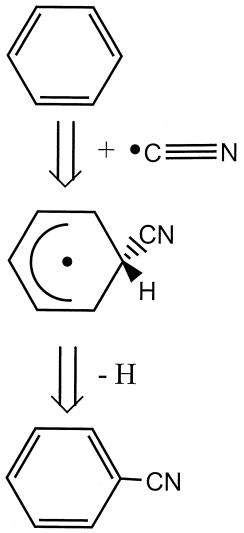

Fig. 27. Schematic representation of the reaction for the reaction $CN(X^2\Sigma^+) + C_6H_6$.

of the cyano radical is mainly localized on the carbon atom making this the more reactive site in radical reactions. Here, the CN radical can interact with the acetylenic carbon–hydrogen σ bond (pathway 1) or the π electron density of two perpendicular π molecular orbitals at the carbon skeleton (pathway 2) (Huang et al., 1999a). Pathway 1 is expected to lead to formation of HCN and the C_2H radical. This reaction, however, is endothermic by 38 kJmol^{-1} and hence can be excluded since the collision energy in our experiments is only 21.1 kJmol^{-1}. In addition, our experimental data support unconditionally a CN vs H exchange to form a product with the molecular formula C_3NH. Therefore, only an attack of the CN radical to the π system is feasible. This pathway is without entrance barrier and form the *cis* and *trans* cyanovinyl radicals, cf Fig. 22. Both complexes are stabilized by about 242 kJmol^{-1} with respect to the reactants. Due to the low barrier of interconversion of the *cis* to the *trans* form and the inherent ultrafast inversion rate constant, the initial concentration of the *cis* vs *trans* population does not influence the chemical reaction dynamics (Chang, 1999). Both complexes can undergo a carbon–hydrogen bond rupture to yield the cyanoacetylene, HCCCN, isomer. Alternatively, a hydrogen atom migration in the initial collision complex to form H_2CCCN radical prior to a H atom emission is found to contribute to about 20% to the HCCCN signal. The experimentally derived reaction energy to form HCCCN of 80–100 kJmol^{-1} is in agreement with the theoretically calculated one of 94 kJmol^{-1}. The formation of a second vinylidene like isomer, C_2CNH, can be excluded, since this reaction is endothermic by 115 kJmol^{-1}.

5.2. $C_2H_4 + CN$ reaction

In analogy to the previous reaction, the CN radical attacks the π molecular orbitals which are situated perpendicular to the C_2H_4 molecular plane, Fig. 23. These pathways are barrierless as well and form the cyanoethyl radical complex. Although the H atom abstraction to form HCN and C_2H_3 is exothermic by 52.5 kJmol^{-1}, the HCN channel could not be detected in our experiments. Based on our center-of-mass angular distribution, the lifetime of the CH_2CH_2CN complex must be longer than its rotational period to account for the symmetric distribution. A symmetric exit transition state is not feasible because the decomposing intermediate belongs to the C_s point group and hence shows no proper *n*-fold rotation axis. Therefore, our experiments prove a hydrogen vs cyano replacement via a long lived complex to form a C_3NH_3 isomer. Here, the reaction energy to the C_2H_3CN of 90–100 kJmol^{-1} as derived from our center-of-mass translational energy distributions agrees with tabulated literature data (Lide 1993). Another isomer, cyanomethylcarbene, NC–C–CH_3, is energetically not accessible in our experiments, and hence cannot be formed in Titan's atmosphere.

5.3. $CH_3CCH + CN$ reaction

The chemical dynamics of CN radicals interacting with methylacetylene are similar to those of the unsubstituted acetylene (Huang et al., 1999b). Again, the barrierless attack to the electronic π system governs the reaction. Since however the alkyne is not symmetric, CN can attack either the α carbon atom (the carbon atom to which the CH_3 group is attached) or the β position. Since the bulky methyl group reduces the cone of acceptance to the α position, CN should attack preferentially the β carbon atom. Further, the β position has a spin density higher than the α atom. This directs the attack of the CN radical to the β position even further to form the *cis* and *trans* $CH_3CC(CN)H$ intermediate, cf Fig. 24. This complex can loose a hydrogen atom from either the CH_3 group or the former acetylenic H atom to form the cyanoacetylene isomer, $H_2CCC(CN)H$, and cyanomethylacetylene, CH_3CCCN, respectively. Based on our center-of-mass functions and TOF data alone we cannot discriminate between these isomers, because they are energetically separated by only 12 kJmol^{-1}. However, our crossed beam experiment employing d_3-methylacetylene, CD_3CCH, emphasizes that two channels are open, i.e. a D atom emission and an H atom release, forming both isomers in our experiments. We like to point out that our collision energy is very different from the actual average collision energy in Titan's atmosphere, and hence we cannot give branching ratios

to the isomer formation at this point. Finally, we like to mention that the high-energy cutoff of the translational energy distribution is consistent with the formation of both isomers and agrees well with the calculated ones to -94 ($H_2CCC(CN)H$) and -106 kJmol^{-1} (CH_3CCCN). We like to stress that we did not find any CH_3 loss channel. This is in coincidence with an attack of the CN radical at the β carbon atom being dominant, since the methyl loss from the *cis*/*trans* collision complexes is endothemic by about 100 kJmol^{-1}. However, due to the unfavorable kinematic relationship of the products, we cannot rule out minor contributions of an α attack and hence formation of cyanoacetylene and a methyl group. This pathway is currently under investigation.

5.4. $H_2CCCH_2 + CN$ reaction

In strong coincidence with the previous reaction, the CN radical attacks the π electron density without entrance barrier with the radical center located at the carbon atom. Here, the formation of the carbon–carbon σ bond can be to the terminal or central carbon atom of the allene molecule. Since the reaction is dominated by large impact parameters similar to the chemical dynamics of the $C(^3P_j) + H_2CCCH_2$ reaction, we conclude that the terminal carbon atom should be attacked preferentially leading to the $H_2CCCH_2(CN)$ intermediate which is stabilized by 233 kJmol^{-1} with respect to the reactants, cf Fig. 25. In addition, if the CN radical forms the new carbon–carbon single bond to the central carbon atom, the intermediate would undergo ring closure followed by hydrogen elimination and formation of a cyanopropene molecule. This pathway, however, is endothermic by about 25 kJmol^{-1}, and hence energetically not accessible in our crossed beam experiments. The initially formed collision complex can lose a hydrogen atom either at the CH_2 or CH_2CN group. Since the transition state of the first pathway is about 31 kJmol^{-1} above the reactant molecules, this mechanism cannot account for our reactive scattering signal. The H loss channel of the CH_2CN site, however, proceeds through a barrier which is located well below the reactants energy by about 63 kJmol^{-1}, and the reaction to the cyanoallene isomer, $HCCCH_2CN$, together with atomic hydrogen is exothermic by ca 90 kJmol^{-1}. This theoretical data is in strong agreement with our experimental range of the reaction exothermicity of 85–90 kJmol^{-1}.

5.5. $H_3CCCCH_3 + CN$ reaction

The dimethylacetylene molecule shows a similar behavior towards reaction of the CN radical as acetylene (1Balucani et al., 1999b). Here, the cyano radical interacts with the π electron density of two perpendicular π molecular orbitals at the carbon skeleton to form a long lived *cis* or *trans* radical complex, cf Fig. 26. In correspondence to the acetylene reaction, this pathway is without an entrance barrier as well, and the reaction dynamics are independent of the initial concentration of the *cis* vs *trans* isomer. Both complexes can undergo a carbon–hydrogen bond rupture to yield the 1,1-cyanomethylallene isomer. The experimental reaction exothermicity of 90 ± 20 kJmol^{-1} is in line with the calculated one of about 80 kJmol^{-1}. Based on the weak reactive scattering signal in the CN vs H exchange and the different kinematics to the CH_3 loss, we calculate data accumulation times of about 1000–1500 h at the center-of-mass angle to obtain a comparable signal to noise ratio as in the H atom loss channel if the branching ratio of both channels is one. This is clearly out of the range of our experimental set up.

5.6. $C_6H_6 + CN$ reaction

The radical–neutral reaction of the cyano radical, $CN(X^2\Sigma^+)$, with benzene, C_6H_6, is initially dominated by long-range dispersion forces (Balucani et al., 1999a). The reaction is barrierless and is governed by an initial attack of the CN radical with the carbon atom to the aromatic π electron density of the benzene molecule to form a C_s symmetric C_6H_6CN collision complex, cf Fig. 27. The center-of-mass angular distributions are forward–backward symmetric and show a peaking at 90°, documenting that the decomposing complex has a life-time longer than its rotational period. Our experimentally determined reaction exothermicity of 80–90 kJmol^{-1} is in good agreement with 94.6 kJmol^{-1} obtained theoretically. We like to stress explicitly that the iso cyanobenzene isomer, C_6H_5NC, is not formed in our experiments and hence in Titan's atmosphere.

6. Summary and conclusion

The crossed molecular beam experiments have been proven an elegant method to unravel the chemical reaction dynamics, involved complexes, and product isomers of radical–neutral reactions of cyano, $CN(X^2\Sigma^+)$, with unsaturated hydrocarbon molecules C_2H_2, C_2H_4, CH_3CCH, H_2CCCH_2, CH_3CCCH_3, and C_6H_6 to form unsaturated nitriles. This is the first direct experimental proof that neutral–neutral reactions of CN radicals with unsaturated hydrocarbons can form nitriles in Titan's atmosphere. All reactions studied in our crossed beam experiments: (a) have no entrance barrier; (b) show an exit barrier well below the energy of the reactant molecules; (c) are exothermic; and (d) proceed through complexes holding lifetimes in the picosecond regime. These characteristics

together with the CN vs H atom exchange channel under well-defined single collision makes this reaction class an ideal candidate to synthesize unsaturated nitriles in Titan's troposphere as well. Here, experimentally detected cyanoacetylene, HCCCN, has been identified unambiguously in Titan. This versatile concept of a cyano radical interacting barrierless with the π electron density of alkenes, alkynes, and aromatic species and the H atom elimination pathway can be even utilized to predict that the hitherto unobserved nitriles CH_3CCCN, C_2H_3CN, $H_2CCCH(CN)$, $H_2CCC(CH_3)CN$, and C_6H_5CN should be present in Titan. Further, we like to stress that no radiative association adduct is formed under single collision conditions as employed in our experiments; however, if we take the denser Titanian atmosphere into account, three-body-reactions are likely to occur as well, and might stabilize the involved collision complexes to yield reactive nitrile radicals in their doublet electronic ground state. These free radicals have unknown spectroscopic properties and could make them responsible for the orange color of the upper atmospheric layers. However, the collision induced stabilization of the intermediate(s) strongly depends on the temperature as well as density profile of Titan's atmosphere, and hence on the mean collision frequency of the complexes with the bath molecules. Therefore, the actual influence on the organic chemistry must be investigated in future reaction networks modeling the chemistry in Titan's atmosphere. Most important, the explicit experimental identification of unsaturated nitriles hitherto unobserved in Titan makes these molecules a unique target for the NASA–ESA Cassini–Huygens mission to Titan. The spacecraft Huygens will carry an IR mapping spectrometer as well as a quadrupole mass spectrometer capable of identifying these isomers in Titan's atmosphere.

Acknowledgements

RIK is indebted to the Deutsche Forschungsgemeinschaft (DFG) for a Habilitation fellowship (IIC1-Ka1081/3-1) and Professor D. Gerlich (Technical University Chemnitz, Germany) for support. The work was supported by Academia Sinica and the Taiwanese Petroleum Corporation.

References

Balucani, N., Asvany, O., Chang, A.H.H., Lin, S.H., Lee, Y.T., Kaiser, R.I., Bettinger, H.F., Schleyer, PvR, Schaefer, H.F. III, 1999a. Crossed-beam reaction of cyano radicals with hydrocarbon molecules I: Chemical dynamics of cyanobenzene (C_6H_5CN; X^1A_1) and perdeutero cyanobenzene (C_6D_5CN; X^1A_1) formation from reaction of $CN(X^2\Sigma^+)$ with benzene, $C_6H_6(X^1A_{1g})$, and d_6-benzene, $C_6D_6(X^1A_{1g})$. J. Chem. Phys. 111, 7457–7471.

Balucani, N., Asvany, O., Chang, A.H.H., Lin, S.H., Lee, Y.T., Kaiser, R.I., Bettinger, H.F., Schleyer, PvR, Schaefer, H.F. III, 1999b. Crossed-beam reaction of cyano radicals with hydrocarbon molecules II: Chemical dynamics of 1,1-cyanomethylallene ($CNCH_3CCCH_2$; X^1A') formation from reaction of $CN(X^2\Sigma^+)$ with dimethylacetylene, CH_3CCCH_3 (X^1A_1'). J. Chem. Phys. 111, 7472–7479.

Butterfield, M.T., Yu, T., Lin, M.C., 1993. Kinetics of CN reactions with allene, butadiene, propylene and acrylonitrile. Chem. Phys. 169, 129–134.

Chang, A.H.H., 1999. Institute of Atomic and Molecular Sciences, unpublished.

Clarke, D.W., Ferris, J.P., 1995. Photodissociation of cyanoacetylene: application to the atmospheric chemistry of Titan. Icarus 115, 119–125.

Clarke, D.W., Ferris, J.P., 1997a. Titan haze: structure and properties of cyanoacetylene and cyanoacetylene–acetylene photopolymers. Icarus 127, 158–172.

Clarke, D.W., Ferris, J.P., 1997b. Symposium of Titan. ESA Special Publication SP 338, 225–230.

Ewan, M.J., Scott, G.B.I., Anicich, V.G., 1998. Ion-molecule reactions relevant to Titan's ionosphere. Inter. J. Mass Spectr. and Ion Processes 172, 209–219.

Fox, J.L., Yelle, R.V., 1997. Hydrocarbon ions in the ionosphere of Titan. Geophysical Res. Lett. 24, 2179–2182.

Griffith, C.A., Owen, T., Miller, G.A., Geballe, T., 1998. Transient clouds in Titan's lower atmosphere. Nature 395, 575–578.

Hidayat, T., Marten, A., Bezard, B., Gautier, D., Owen, T., Matthews, H.E., Paubert, G., 1998. Millimeter and submillimeter heterodyne observations of Titan: the vertical profile of carbon monoxide in its stratosphere. Icarus 133, 109–133.

Hidayat, T., Marten, A., Bezard, B., Owen, T., Matthews, H.E., Paubert, G., 1997. Millimeter and submillimeter heterodyne observations of Titan: retrieval of the vertical profile of HCN and the $^{12}C/^{13}C$ ratio. Icarus 126, 170–182.

Huang, L.C.L., Lee, Y.T., Kaiser, R.I., 1999a. Crossed beam reaction of the cyano radical, $CN(X^2\Sigma^+)$,with acetylene, $C_2H_2(X^1\Sigma_g^+)$: observation of cyanoacetylene, HCCCN ($X^1\Sigma^+$). J. Chem. Phys. 110, 7119–7122.

Huang, L.C.L., Osamura, Y., Balucani, N., Lee, Y.T., Kaiser, R.I., 1999b. Crossed beam reaction of the cyano radical, $CN(X^2\Sigma^+)$, with methylacetylene, CH_3CCH (X^1A_1): observation of cyanopropyne, CH_3CCCN (X^1A_1), and cyanoallene, $H_2CCCHCN$ (X^1A'). J. Chem. Phys. 111, 2857–2860.

Ip, W.H., 1990. Titan's upper ionosphere. Astrop. J. 362, 354–363.

Kaiser, R.I., Suits, A.G., 1995. A high-intensity, pulsed supersonic carbon source with $C(^3P_j)$ kinetic energies of 0.08–0.7 eV for crossed beam experiments. Rev. Sci. Instr. 66, 5405–5410.

Kaiser, R.I., Ting, J., Huang, L.C.L., Lee, Y.T., Chan, H., Stranges, D., Gee, D., 1999. A versatile source to produce high intensity, pulsed supersonic radical beams for crossed beams experiments — the cyano radical $CN(X^2\Sigma^+)$, as a case study. Rev. Sci, Instr. 70, 4185–4191.

Karkoschka, E., 1994. Spectrophotometry of the Jovian planets and Titan at 300- to 1000-nm wavelength: the methane spectrum. Icarus 111, 174–192.

Keller, C.N., Anicich, V.G., Cravens, T.E., 1998. Model of Titan's ionosphere with detailed hydrocarbon ion chemistry. Planet. Space Sci. 46, 1157–1174.

Kostiuk, T., Fast, K., Livengood, T.A., Goldstein, J., Hewagama, T., Buhl, D., Espenak, F., Ro, K.H., 1997. Ethane abundance on Titan. Planet. Space Sci. 45, 931–939.

Lara, L.M., Lorenz, R.D., Rodrigo, R., 1994. Liquids and solids on the surface of Titan: results of a new photochemical model. Planet. Space Sci. 42, 5–14.

Lara, L.M., Rodrigo, R., Coustenis, A., Lopez-Moreno, J.J., Chassefiere, E., 1991. Neutral composition of Titan's atmosphere. A theoretical model. Proceedings Symposium on Titan 338, 137–146.

Lellouch, E., 1990. Atmospheric models of Titan and Triton. Ann. Geophy. 8, 653–660.

Letourneur, B., Coustenis, A., 1993. Titan's atmospheric structure from Voyager 2 infrared spectra. Planet. Space Sci. 41, 593–602.

Levine, R.D., Bernstein, R.B., 1987. Molecular Reaction Dynamics and Chemical Reactivity. Oxford University Press, Oxford.

Lichtin, D.A., Lin, M.C., 1985. Kinetics of CN radical reactions with selected molecules at room temperature. Chem. Phys. 96, 473–482.

Lichtin, D.A., Lin, M.C., 1986. Temperature dependence of the CN radical reactions with C_2H_2 and C_2H_4. Chem. Phys. 104, 325–330.

Lide, D.R., 1993. Handbook of Chemistry and Physics. CRC Press, Boca Raton.

Lorenz, R., McKay, C.P., Lunine, J.I., 1997. Photochemically driven collapse of Titan's atmosphere. Science 275, 642–644.

Lunine, J.I., Lorenz, R.D., Hartmann, W.K., 1998. Some speculations on Titan's past, present and future. Planet. Space Sci. 46, 1099–1107.

Nagy, A.F., Cravens, T.E., 1998. Titan's ionosphere: a review. Planet. Space Sci. 46, 1149–1155.

Nascimento, L.F.C., Mota, R.P., Valenca, G.P., Teixeira, J.C., Algatti, M.A., Honda, R.Y., Bortoleto, J.R.R., 1998. An N_2:CH_4:H_20 DC glow discharge plasma probed by optical and electric techniques: significance to the radiation chemistry of Titan's upper atmosphere in the presence of meteoritic water. Planet. Space Sci. 46, 969–974.

North, S.W., Fei, R., Sears, T.J., Hall, G.E., 1997. CN radical reaction rate measurements by time-resolved FM spectroscopy. Inter. J. Chem. Kin. 29, 127–129.

Raulin, F., Accaoui, B., Razaghi, A., Dang-Nhu, M., Coustenis, A., Gautier, D., 1990. Infrared spectra of gaseous organics: application to the atmosphere of Titan — II. Infrared intensities and frequencies of C_4 alkanenitriles and benzene. Spectrochimica Acta 46A, 671–683.

Raulin, F., Coll, P., Gazeau, M.C., Sternberg, R., Bruston, P., Israel, G., Gautier, D., 1998. An exobiological view of Titan and the Cassini–Huygens mission. Adv. Space Res. 22, 353–362.

Rowe, B.R., Parent, D.C., 1995. Techniques for the study of reaction kinetics at low temperatures: application to the atmospheric chemistry of Titan. Planet. Space Sci. 43, 105–114.

Seki, K., He, M., Liu, R., Okabe, H., 1996. Photochemistry of cyanoacetylene at 193.3 nm. J. Phys. Chem. 100, 5349–5353.

Smith, I.W.M., Sims, I.R., Rowe, B.R., 1997. Gas-phase reactions at low temperatures: towards absolute zero. Chem. Eur. J. 3, 1925–1928.

Tanguy, L., Benzard, B., Marten, A., Gautier, D., Gerard, E., Paubert, G., Lecacheux, A., 1990. Stratospheric profile of HCN on Titan from millimeter observations. Icarus 85, 43–57.

Thompson, W.R., Henry, T.J., Schwartz, J.M., Khare, B.N., Sagan, C., 1991. Plasma discharge in N_2+CH_4 at low pressures: experimental results and applications to Titan. Icarus 90, 57–73.

Yang, D.L., Yu, T., Wang, N.S., Lin, M.C., 1992. CN radical reactions with selected olefins in the temperature range 174–740 K. Chem. Phys. 160, 317–325.